


Review

Isolating Fe-O₂ Intermediates in Dioxygen Activation by Iron Porphyrin Complexes

Xiaoyan Lu ^{*}, Shuang Wang and Jian-Hua Qin

College of Chemistry and Chemical Engineering, Luoyang Normal University, Luoyang 471934, China; dyyxqy1990@163.com (S.W.); jh_q128105@126.com (J.-H.Q.)

* Correspondence: zklxiaoyan@163.com

Abstract: Dioxygen (O₂) is an environmentally benign and abundant oxidant whose utilization is of great interest in the design of bioinspired synthetic catalytic oxidation systems to reduce energy consumption. However, it is unfortunate that utilization of O₂ is a significant challenge because of the thermodynamic stability of O₂ in its triplet ground state. Nevertheless, nature is able to overcome the spin state barrier using enzymes, which contain transition metals with unpaired *d*-electrons facilitating the activation of O₂ by metal coordination. This inspires bioinorganic chemists to synthesize biomimetic small-molecule iron porphyrin complexes to carry out the O₂ activation, wherein Fe-O₂ species have been implicated as the key reactive intermediates. In recent years, a number of Fe-O₂ intermediates have been synthesized by activating O₂ at iron centers supported on porphyrin ligands. In this review, we focus on a few examples of these advances with emphasis in each case on the particular design of iron porphyrin complexes and particular reaction environments to stabilize and isolate metal-O₂ intermediates in dioxygen activation, which will provide clues to elucidate structures of reactive intermediates and mechanistic insights in biological processes.

Keywords: oxygen activation; iron porphyrin complexes; Fe-O₂ intermediates; enzymes; superoxo



Citation: Lu, X.; Wang, S.; Qin, J.-H.

Isolating Fe-O₂ Intermediates in Dioxygen Activation by Iron Porphyrin Complexes. *Molecules* **2022**, *27*, 4690. <https://doi.org/10.3390/molecules27154690>

Academic Editor: Ana Margarida Gomes da Silva

Received: 15 June 2022

Accepted: 18 July 2022

Published: 22 July 2022

Publisher's Note: MDPI stays neutral with regard to jurisdictional claims in published maps and institutional affiliations.



Copyright: © 2022 by the authors. Licensee MDPI, Basel, Switzerland. This article is an open access article distributed under the terms and conditions of the Creative Commons Attribution (CC BY) license (<https://creativecommons.org/licenses/by/4.0/>).

1. Introduction

Dioxygen (O₂) is a primary component of the atmosphere and is essential in life processes. The biochemical processes that mediate the highly exergonic four-electron reduction of oxygen to water with an enthalpy change of −80 kcal/mol provide the energy for sustaining aerobic organisms [1]. With a redox potential of 0.815 V vs. NHE in water at pH 7 and 25 °C, the overall four-electron reduction of O₂ is thermodynamically favorable [2]. However, the activation of O₂ is kinetically hindered because of its triplet ground state, which makes direct combination of O₂ with typical organic compounds spin-forbidden [3–5]. To overcome this difficulty, nature has evolved a wide variety of enzymes, which contain transition metals (e.g., Fe, Mn, Cu, and Co) with unpaired *d*-electrons facilitating the activation of O₂ by metal coordination, to carry out various vital biological processes [6]. The function of transition metals is not only to serve as O₂ binding sites for transport, but also to serve as active centers where they can carry out multi-electron redox process that ultimately result in the incorporation of oxygen in organic substrates [7].

The binding of O₂ to ferrous porphyrins constitutes the first step in the biological function of a majority of heme enzymes. Processes involving cleavage of the O-O bond require proteins with specific structural and chemical features designed to facilitate O₂ activation [7]. Cytochrome P450, one of the important dioxygen-activating heme enzymes, has thrown light on the catalytic cycles of O₂ activation and oxygen transfer reactions [8–12]. The consensus mechanism for O₂ activation by cytochrome P450 is shown in Figure 1 [9]. The spin-state of the six-coordinate ferric complex at the active site in cytochrome P450 is low-spin, which turns into a high-spin five-coordinate ferric complex upon binding of the substrate to remove the aqua ligand. One-electron reduction of this high-spin five-coordinate ferric species generates a high-spin ferrous compound, which is quite activated

for O₂ binding to give an iron (III)-superoxo intermediate. Then, a second one-electron reduction occurs to form an iron (III)-peroxo complex, which turns into an iron (III)-hydroperoxo complex (Compound 0) upon protonation. Heterolytic cleavage of the O-O bond of Compound 0 produces an iron (IV)-oxo porphyrin π -cation radical intermediate (Compound I) and one molecule of water [10]. The generally accepted mechanism for C-H bond activation of alkanes by Compound I is the “oxygen-rebound” mechanism [11], where the H-atom of the substrate is abstracted by Compound I to generate an iron (IV)-hydroxo species and a carbon radical that recombine to form alcohol and the ferric heme resting state.

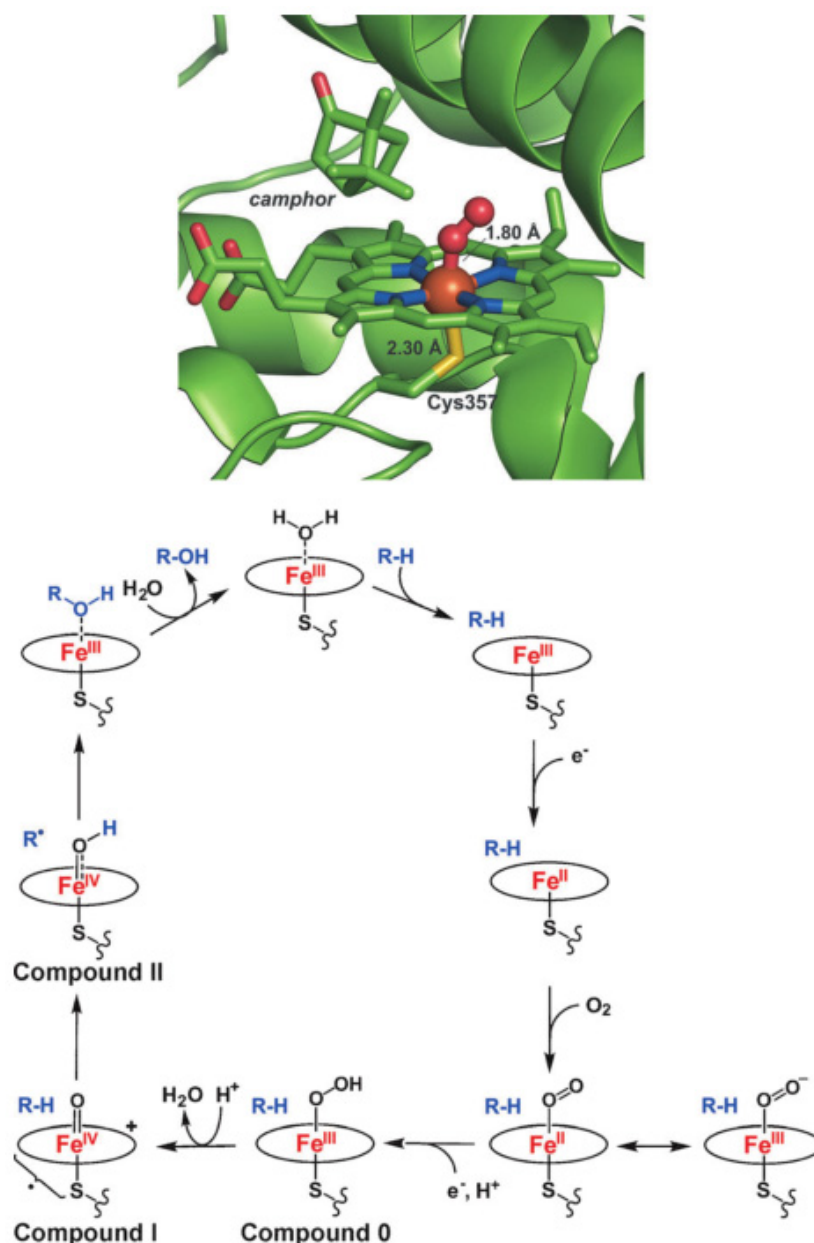


Figure 1. O₂ bound to the ferrous heme in the active site of cytochrome P450 (**top**); the catalytic cycle of cytochrome P450 (**bottom**). Reprinted with permission from Ref. [9]. Copyright 2014, WILEY-VCH Verlag GmbH.

Metal-dioxygen species are crucial intermediates in the O₂ activation cycle of metalloenzymes, and their redox reactivities are modulated by the nature of metal ions and ligands in metalloenzymes [13–26]. In living organisms, the metalloporphyrin sites are sur-

rounded by the protein superstructure, which is conducive to avoiding the involvement of metalloporphyrin active sites in unwanted side reactions [13,15,27–30]. However, the complexity of the surrounding protein superstructure restricts access to the metalloporphyrin active sites, resulting in the big challenge in studying the intermediates in O_2 activation by metalloenzymes. To deal with this big challenge, the last several decades have seen numerous researchers turn towards the development of molecular model complexes with heme and nonheme ligands that mimic the local coordination environment of the active site in enzymes [31–37]. Due to the simplicity of molecular model complexes, the metal–dioxygen intermediates can be stabilized and directly characterized using current techniques.

The heme cofactor, being made of an iron-bound porphyrin, is at the active site of many metalloproteins and carries out oxygen transport, storage, electron transfer, and oxygenation reactions [38–40]. Thus, due to the bioavailability of iron porphyrins in nature, iron porphyrins have been well-studied. The successfully isolated and characterized metal–dioxygen intermediates in iron porphyrin complexes can make us understand physicochemical properties of the metalloenzymes and study the correlation of the structural properties of the active sites and their reactivities in well-controlled environments. In this review, we focus on a few examples of these advances with emphasis in each case on the particular reaction conditions and design of iron porphyrin complexes to stabilize and isolate Fe– O_2 intermediates in O_2 activation, which will provide clues to elucidate structures of reactive intermediates and mechanistic insights in biological processes for the design of effective catalysts.

2. Nature of Iron–Dioxygen Bond

The structural and electronic properties of iron–dioxygen adduct are crucial for understanding the O_2 activation in heme proteins and metalloporphyrins. However, a controversy exists over the nature of Fe– O_2 bonds in hemoproteins and metalloporphyrins. As early as 1936, Pauling and Coryell reported that oxygenated hemoglobin (oxy-Hb) was diamagnetic and proposed that dioxygen was bound to iron in a bent, end-on mode [41,42]. This geometric feature was confirmed by an oxy–ferrous model compound prepared by Collman and co-workers and by crystal structures of oxy-Hb reported by Shaanan, respectively [43,44]. These pioneering works suggest that the electronic structure of oxy-Hb is described as a Fe^{II}– O_2 adduct, where complete electron transfer from O_2 to iron has not taken place (Figure 2) [45].

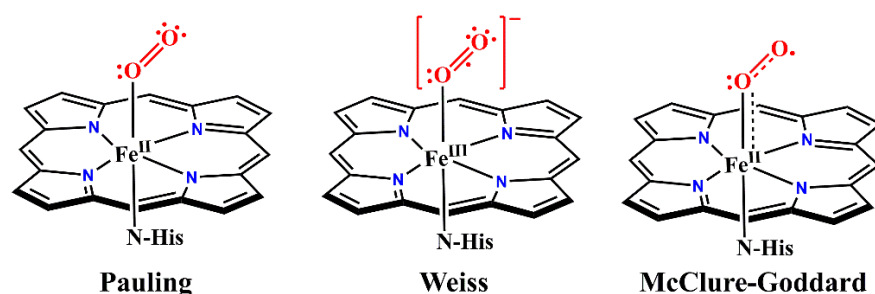


Figure 2. Three models of the iron–dioxygen bond. Pauling model: Low-spin ($S = 0$) Fe^{II} with singlet O_2 ; Weiss model: Low-spin ($S = 1/2$) Fe^{III} antiferromagnetically coupled to an $O_2^{\bullet-}$; McClure-Goddard model (ozone model): Intermediate-spin ($S = 1$) Fe^{II} antiferromagnetically coupled to triplet O_2 . Reprinted with permission from Ref. [45]. Copyright 2013 American Chemical Society.

In contrast, Weiss and co-workers propose that the Fe– O_2 species would be best described as a ferric superoxide complex, where the observed diamagnetism of oxy-Hb is explained by the antiferromagnetic coupling between a doublet superoxide anion $O_2^{\bullet-}$ ($S = 1/2$) and a low-spin Fe^{III} ($S = 1/2$) to result in an overall spin of $S = 0$ (Figure 2) [45]. Mössbauer studies have lent support to the Weiss model. The Mössbauer parameters of oxy-Hb with isomer shift $\delta = 0.2–0.3$ mm/s and quadrupole splitting $\Delta E_Q = 2.00–2.20$ mm/s,

first measured by Lang and co-workers, are in good agreement with a low-spin ferric center [46,47]. Sharrock and co-workers have given close parameters for oxygenated reduced P450cam, which are $\delta = 0.3159$ mm/s and $\Delta E_Q = 2.15$ mm/s [48]. Collman and co-workers present infrared data on Fe-O₂ adducts in “picket-fence” porphyrin ($\alpha,\alpha,\alpha,\alpha$ -tetrapivalamidophenylporphyrin, $\alpha,\alpha,\alpha,\alpha$ -T pivPP) complexes with 1-methylimidazole (1-MeIm) and 1-tritylimidazole (1-tritylIm) as axial bases. The O₂ vibration of Fe-O₂ adducts are achieved using difference techniques between ¹⁶O₂, ¹⁸O₂, ¹⁶O-¹⁸O, and NO with a Fourier transform infrared spectrometer. They compare the obtained ν_{O_2} with known M-O₂ (M = Fe, Co, Cr, and Ti) complexes and concluded that Fe-O₂ adducts are best described as Fe^{III}-O₂^{•−} [49]. The Fe^{III}-O₂^{•−} model obtained further support by resonance Raman spectroscopic studies, where a ferric center was indicated by the oxidation state marker band of oxy-Hb ($\nu = 1377$ cm^{−1}) [50–52].

The third model (“Ozone model”), initially suggested by McClure and refined by Goddard, presents the oxy-form electronic structure as an antiferromagnetically coupled intermediate spin ferrous center ($S = 1$) and a triplet dioxygen ligand ($S = 1$) [53–56]. In a recent report, Haumann and co-workers apply the X-ray spectroscopic techniques and computations on O₂-bound hemes in myoglobin (Mb) and hemoglobin (Hb) and in porphyrin complexes at 20–260 K [57]. Based on the results, they describe an essentially ferrous, intermediate-spin iron in an ozone-like configuration in O₂-bound heme compounds, supporting the McClure–Goddard model.

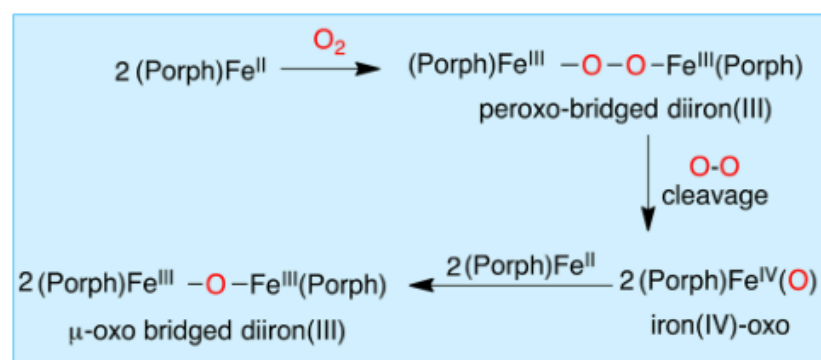
Using generalized valence bond (GVB) wave function, Shaik and co-workers have presented Fe-O₂ bonding that includes a σ (Fe–O) bond and a π (Fe–O₂) bond between d_{yz} (Fe) and π_{\perp}^* (O₂) with quite small delocalization tails [58]. Thus, they propose one electron transferred from Fe^{II} center to O₂ to form Fe^{III} center and superoxo O₂^{•−}, that is, the Weiss bonding model. Furthermore, H-bonding capability and the polarity of the protein is able to modulate the O₂ affinity to consolidate the character of Fe^{III}-O₂^{•−}. Although Fe–O₂ follows the Fe^{III}-O₂^{•−} bonding model from the GVB wave function, the pure VB analysis showed a mixing of the other two models with the Pauling model being the least important, and axial ligands and protein host determined the nature of the Fe–O₂ bonding. In addition, an iron L-edge X-ray absorption spectroscopy study of a ferric-superoxo “picket fence” porphyrin with 1-methylimidazole (1-MeIm) axial ligand, [Fe(O₂)(1-MeIm)($\alpha,\alpha,\alpha,\alpha$ -T pivPP)], also strongly supports the key impact of local environment on the nature of Fe–O₂ bonding [45]. Interestingly, in a recent work of Sarangi and co-workers, the solution-state structure of oxy-Hb is best described as Fe^{III}-O₂^{•−} (Weiss model); however, the crystalline oxy-Hb favors (Fe^{II}–O₂) (Pauling model) through theoretical and spectroscopic studies. This surprising change of electronic configuration with environment is in favor of the multiconfigurational description [59]. Even though the current findings of oxy-heme intermediates are unable to give a simple explanation for their electronic structures, notable recent work has presented the necessity of electron transfer from the iron center to the dioxygen moiety so as to produce oxy-heme-type intermediates, emphasizing the unambiguous validity of the Weiss model [60–64].

3. Strategies to Stabilize Iron–Dioxygen Intermediates in O₂ Activation

3.1. Sterically Hindered Metal Porphyrin Complexes

Biomimetic synthetic iron porphyrin complexes, which have the same core structure as the heme cofactor, are perfect models to study the O₂ activation. However, a major hurdle presents in simple iron (II) porphyrin complexes, which are facile to undergo bimolecular condensation to form μ -oxo-bridged diiron (III) complexes upon reacting with O₂ [13]. The single-atom bridged binuclear complexes have been considered as catalytically inert for a long time. However, Sorokin’s group synthesized and spectroscopically characterized a variety of μ -oxo-bridged and μ -nitrido-bridged complexes, which provided superior catalytic properties [65–67]. For example, employing μ -nitrido-bridged diiron *meso*-tetraphenylporphyrin [(TPP)Fe^{III}(μ -N)Fe^{IV}(TPP)], they prepared a highly reactive intermediate, Fe(IV)(μ -N)Fe(IV)(=O) tetraphenylporphyrin cation radical species, which

exhibited a very high activity for C–H activation towards alkanes, even including the strongest C–H bond of methane [65]. Until the 1980s, the mechanism for the bimolecular condensation was fully described as shown in Scheme 1 [68], in which the autoxidation proceeds via a peroxo-bridged diiron(III) and the Fe^{IV}(O) intermediates [68–72]. Encouragingly, this hurdle has been partially overcome through introduction of sterically hindered substituents onto porphyrin scaffolds, which prevent bimolecular condensation reactions and enable isolation and thorough characterization of heme-O₂ adducts [73–80].



Scheme 1. Dioxygen-mediated autoxidation mechanism for ferrous porphyrin complexes. Reprinted with permission from Ref. [68]. Copyright 2016 American Chemical Society.

Much progress in stabilizing an Fe–O₂ moiety as a functional mimic of an O₂-bound heme system has been made with sterically protected porphyrin scaffolds such as “picket-fence” porphyrins, which is first implemented by Collman and co-workers to prevent the irreversible bimolecular condensation of iron(II) porphyrin complexes to form μ-oxo-bridged diiron(III) species upon reacting with O₂. In 1973, Collman and co-workers construct a “picket fence” porphyrin, whose steric bulk on one side creates a nonprotic cavity for the coordination of O₂ while also protecting O₂ from bimolecular reactions [60]. *meso*-Tetra(*o*-aminophenyl)porphyrin (H₂TamPP) is synthesized by SnCl₂ reduction of *meso*-tetra(*o*-nitrophenyl)porphyrin and separated into its four atropisomers. Then, the slowest moving isomer is isolated in 12% yield and its configuration frozen by formation of the amide, *meso*-tetra($\alpha,\alpha,\alpha,\alpha$ -*o*-pivalamidephenyl)porphyrin ($\alpha,\alpha,\alpha,\alpha$ -H₂TpivPP) [77]. Treatment with FeBr₂ affords purple crystals of [Fe^{III}Br($\alpha,\alpha,\alpha,\alpha$ -TpivPP)], which is then reduced to give [Fe^{II}($\alpha,\alpha,\alpha,\alpha$ -TpivPP)]. [Fe^{II}($\alpha,\alpha,\alpha,\alpha$ -TpivPP)] reacted with 1-methylimidazole (1-MeIm) giving crystalline, diamagnetic complex, [Fe^{II}(1-MeIm)₂($\alpha,\alpha,\alpha,\alpha$ -TpivPP)], **1** (Figure 3). The first determination of the geometry of 1:1 coordinated dioxygen in an Fe(II) model compound, [Fe(O₂)(1-MeIm)($\alpha,\alpha,\alpha,\alpha$ -TpivPP)], **1-O₂**, is then crystallized by dropwise heptane addition to the benzene solution of **1** exposed to O₂ (1 atm) in the presence of a small excess of 1-MeIm. **1-O₂** has a similar Mössbauer spectrum to oxyhemoglobin and otherwise closely resembles biologically important heme-protein molecules. However, crystals of **1-O₂** are too small to afford good x-ray intensity data. Hearteningly, soon afterwards, they find that toluene replaces benzene as a solvent to yield large crystals of **1-O₂**, which allows to analyze its structure in detail [44]. Crystal structure displays that **1-O₂** has four pivalamido groups on one side of the porphyrin forming a hydrophobic pocket of 5.4 Å depth, which encloses coordinated dioxygen in an “end-on” model. The end-on bent (Fe–O–O angle ~126°) dioxygen ligand is in close agreement with Pauling’s 1964 model for describing oxy-Hb electronic structure [41]. **1-O₂** crystallizes in two space groups with four molecules in each unit cell, where the Fe–O–O plane is either parallel or perpendicular to the trans-axial imidazole plane. Thus, significant distortions result. The structure indicates O–O distances of 1.23(8) and 1.26(8) Å, which are consistent with that of coordinated superoxides [81].

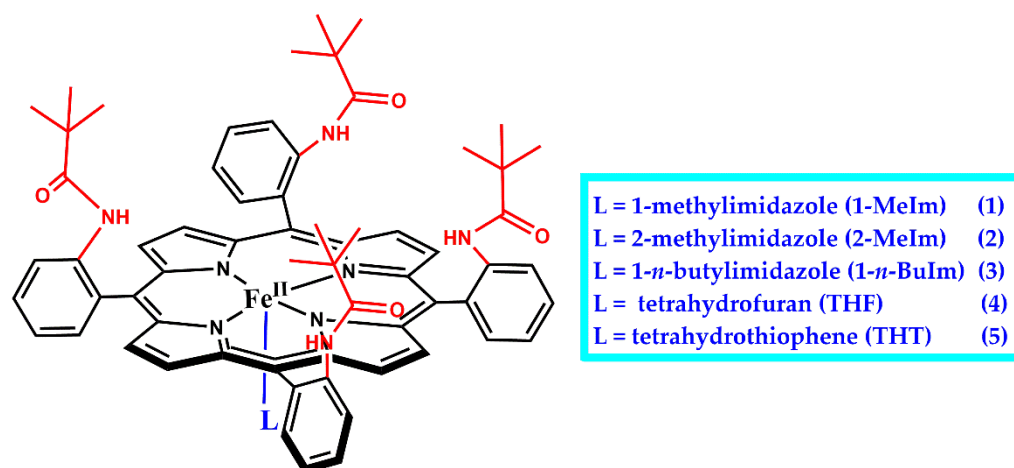


Figure 3. Chemical structures of iron(II) complexes of “picket-fence” porphyrin with substituted axial ligands, $[\text{Fe}^{\text{II}}(\text{L})(\alpha,\alpha,\alpha,\alpha\text{-TpivPP})]$.

Collman and co-workers replace 1-MeIm with 2-methylimidazole (2-MeIm), and a five-coordinate complex $[\text{Fe}(2\text{-MeIm})(\alpha,\alpha,\alpha,\alpha\text{-TpivPP})(\text{C}_2\text{H}_5\text{OH})]$ (**2**) is synthesized. The six-coordinate dioxygen adduct of **2**, $[\text{Fe}(\text{O}_2)(2\text{-MeIm})(\alpha,\alpha,\alpha,\alpha\text{-TpivPP})]$ (**2-O₂**) is then prepared by exposing crystals of **2** for 3 days at 20 °C to 1–2 atm of O₂, which is saturated with ethanol vapor [81–83]. The 2-MeIm ligand leads to lengthened axial bonds relative to the sterically undemanding 1-MeIm ligand, and the sum of the Fe-N_{im} and Fe-O separations is 4.005 Å in **2-O₂**, but only 3.813 Å in **1-O₂**. For **2-O₂**, the compromise between minimum destabilizing nonbonding contacts and maximum bonding leads to the iron atom remaining 0.086 Å out of the plane toward the imidazole ligand, in contrast to **1-O₂**, where the iron atom is displaced only 0.030 Å toward the O₂ ligand [44,76]. The porphyrinato-dioxygen nonbonding contacts are not significantly different between **2-O₂** and **1-O₂**. Further adjustment for the steric hindrance of the 2-MeIm group is made by significant buckling of the porphyrinato skeleton, that is, the mean displacement from the least-squares plane is 0.066 Å in **2-O₂**, which is 0.010 Å larger than that in **1-O₂**. The O₂ ligand is again found coordinated in the bent, end-on fashion, with four-fold disorder.

Suppression of irreversible oxidation was so successful with $[\text{Fe}^{\text{II}}(\alpha,\alpha,\alpha,\alpha\text{-TpivPP})]$ when 1-MeIm and 2-MeIm as the axial ligands that $[\text{Fe}^{\text{II}}(\alpha,\alpha,\alpha,\alpha\text{-TpivPP})]$ with other axial bases has also been examined to isolate the dioxygen adducts by Collman and co-workers (Figure 3). Benzene solutions of $[\text{Fe}^{\text{II}}(\alpha,\alpha,\alpha,\alpha\text{-TpivPP})]$ prepared under nitrogen and containing an excess of 1-*n*-BuIm are treated with O₂ (1 atm) at 25 °C, which results in the visible spectral changes to form dioxygen adduct, $[\text{Fe}(\text{O}_2)(1\text{-}n\text{-BuIm})(\alpha,\alpha,\alpha,\alpha\text{-TpivPP})]$ (**3-O₂**). The Mössbauer and magnetic data show that **3-O₂** is essentially diamagnetic, like oxy-Hb [42,84]. **3-O₂** does not show IR or Raman absorptions at room temperature, but at −175 °C, its IR spectrum reveals a remarkably sharp band at 1385 cm^{−1}, which was assigned as dioxygen vibration (ν_{O_2}). Reduction of $[\text{Fe}^{\text{III}}\text{Br}(\alpha,\alpha,\alpha,\alpha\text{-TpivPP})]$ in THF produces crystals [85] of high-spin $[\text{Fe}^{\text{II}}(\text{THF})(\alpha,\alpha,\alpha,\alpha\text{-TpivPP})]$ (**4**) at 25 °C where only one THF is presumed to coordinate to iron(II). This assumption is consistent with the behavior of the simple ferrous complexes in THF solution [86]. In the solid state, **4** reversibly absorbs 1 equiv. of O₂ to yield a reported paramagnetic ($\mu_{\text{eff}} = 2.4$ BM) dioxygen adduct, $[\text{Fe}(\text{O}_2)(\text{THF})(\alpha,\alpha,\alpha,\alpha\text{-TpivPP})]$ (**4-O₂**). Coordinated O₂ can be removed from solid **4-O₂** in vacuo, and the reversible solid-state oxygenation is followed through several cycles by monitoring changes in magnetic susceptibility. However, the complex is later shown by Mössbauer spectroscopy to be diamagnetic [84,85]. In addition, Collman and co-workers also observe the formation of dioxygen adduct (**5-O₂**) upon exposure $[\text{Fe}^{\text{II}}(\text{THT})(\alpha,\alpha,\alpha,\alpha\text{-TpivPP})]$ (**5**; THT: tetrahydrothiophene) to O₂. The Mössbauer spectrum of **5-O₂** was found to be quite similar to that of **1-O₂**.

3.2. Secondary Coordination Sphere Interactions

The secondary coordination sphere interactions are another promising strategy for building discrete molecules with improved O₂ activation properties and increasing the stability of the O₂ intermediates. “Single-coronet” model system (6) designed by Naruta and co-workers is such a compound, which is constitutive of highly sterically bulky substituted dinaphthalene moieties that establish a hydrophobic environment around the Fe center, while providing –OH for secondary coordination sphere interactions (Figure 4). As presented in biological heme centers [87,88], this uniquely designed architecture has been reported to mediate the Fe–O₂ affinities to increase the stabilities of Fe–O₂ adducts [89,90], wherein hydrogen-bonding interactions on Fe–O₂ adducts result in the huge change in affinity (Figure 5) [89,91].

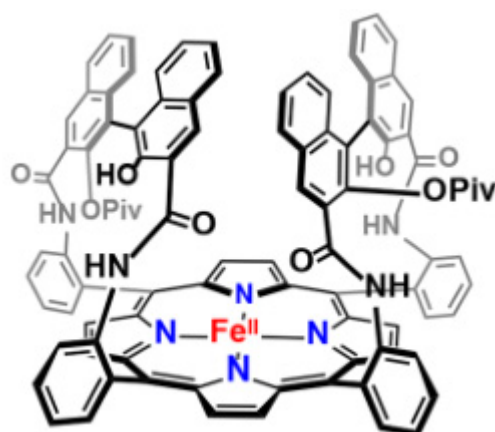


Figure 4. “Single-coronet” model system designed by Naruta and co-workers. Reprinted with permission from Ref. [15]. Copyright 2018, American Chemical Society.

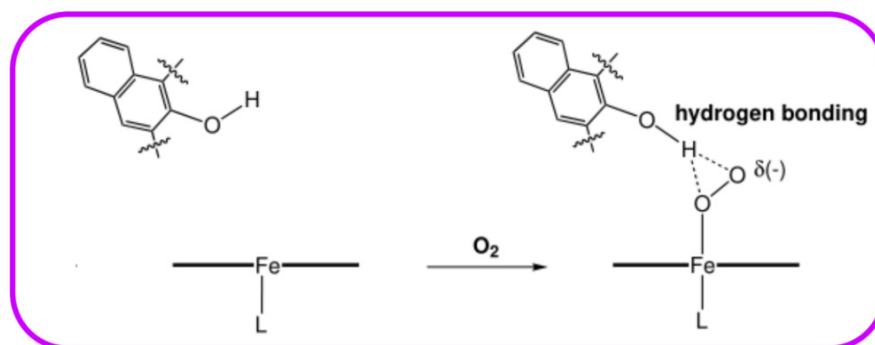


Figure 5. Stabilization of Fe–O₂ species through hydrogen-bonding interactions resulting from hydroxylated naphthyl functionalities in “coronet” model systems. Reprinted with permission from Ref. [90]. Copyright 2003, WILEY-VCH Verlag GmbH.

In a subsequent study, Naruta and co-workers also prepare “twin-coronet” ligand platforms, which introduce a tethered imidazole (7) or pyridine (8) to the porphyrinate periphery (Figure 6) [90]. The dioxygen adducts (7–O₂, 8–O₂) of these “twin-coronet” models reveal striking stability with half-lives up to several days in toluene at 25 °C. They suggested that the remarkable stability of the Fe–O₂ adducts resulted from the hydrogen bonding to bound O₂ moieties in the secondary coordination sphere in 7–O₂ and 8–O₂. The resonance Raman (rR) spectra of 7–O₂ and 8–O₂ showed $\nu(\text{Fe–O})$ stretching centered at 586 cm^{−1} and 583 cm^{−1}, respectively, which are higher than those of other Fe–oxy species in model systems [92–94] and biological examples [95,96], resulting from hydrogen-bonding interactions between the O₂ moiety and the –OH of the coronet ligand. The hydrogen-bonding interactions are further proved by infrared (IR) spectroscopic features of 7–O₂ and

8-O₂, where the O–H IR stretching frequency of the ligand significantly loses intensity compared to **7** and **8**. Thus, the “twin-coronet” model systems are able to mediate O₂ affinity and shed light on the importance of secondary coordination sphere interactions, which could explain how O₂ activation occurs in enzyme systems.

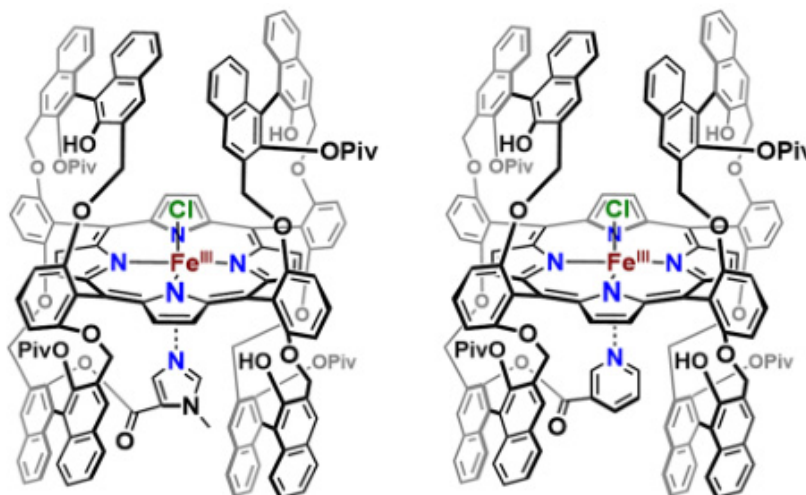


Figure 6. “Twin-coronet” model systems with tethered axial N-based ligands. Reprinted with permission from Ref. [15]. Copyright 2018, American Chemical Society.

3.3. Cryogenic Temperature

Designing model systems that can precisely mimic the electronic and geometric characteristics of iron–dioxygen adducts that form within biological heme-containing proteins remains a huge challenge for biomimetic chemists [58,72]. Heme iron(III)-superoxo intermediates can be readily produced when iron(II) porphyrin complexes are exposed to O₂. Nevertheless, formed iron(III)-superoxo intermediates are too unstable to be isolated or observed, resulting in only a handful of oxyheme models found to date [97,98]. The cryogenic temperature technique is a very effective way to observe and isolate iron–dioxygen adducts, because the decomposition of iron–dioxygen adducts is retarded and the bimolecular reaction to form μ -peroxo derivatives is remarkably slowed at low temperature [60,73].

Karlin and co-workers report several examples of heme–superoxo complexes, which are characterized at cryogenic temperature [99–102]. As early as in 1999, when Karlin and co-workers carry out the synthesis of an iron-copper dinuclear active site, [(F₈TPP)Fe^{III}-O-Cu^{II}(MePY2)]⁺ [F₈TPP = tetrakis(2,6-difluorophenyl)porphyrinate; MePY2 = *N,N*-bis[2-(2-pyridyl)ethyl]-methylamine], they observe a transient iron(III)-superoxo species, [(F₈TPP)Fe^{III}(O₂^{•-})] (**9-O₂**), at cryogenic temperature by stopped-flow experiments (Figure 5). Adding O₂ to the acetone solution including [(MePY2)Cu^I(MeCN)]⁺ and [(F₈TPP)Fe^{II}] (**9**) at −90 °C leads to the generation of **9-O₂** with characteristic absorption band at $\lambda_{\text{max}} = 535$ nm within 1 ms, which is also observed when **9** alone reacts with O₂ in THF. However, the low-temperature stopped-flow kinetic experiments exhibit that **9-O₂** is very unstable and transforms into a new species with distinct absorption bands at 560 nm within 1 s. Soon afterward, Karlin and co-workers reported the detailed characterization of **9-O₂** under various conditions of solvent and temperature using multinuclear NMR and UV-visible spectroscopies in 2001 [100]. In coordinating solvents, including THF, propionitrile, and acetone, **9** reacts with O₂ at cryogenic temperature to generate a quite stable iron(III)-superoxo species, [(S)(F₈TPP)Fe^{III}(O₂^{•-})] (**9-S-O₂**) (S = solvent) (Figure 7). A full reversible phenomenon is observed by benchtop UV-visible spectroscopy, the kinetics and thermodynamics of formation of **9-S-O₂** is determined by stopped-flow spectrophotometry, and Fe/O₂ stoichiometry of 1:1 is determined by dioxygen-uptake manometry at 193 K. The ²H NMR spectrum of **9-THF-O₂** with deuterated β -pyrrolic positions gives evidence of a diamagnetic low-spin iron center with $\delta_{\text{pyrrole}} = 8.9$ ppm, confirming the presence of a 6C

Fe^{III} center in the superoxo complex, wherein the diamagnetism results from the antiferromagnetic coupling of the low-spin iron(III) ion with the superoxo radical anion [49,73]. The ^{19}F -NMR spectrum of **9-THF-O₂** reveals two identical integrations of F resonances at -111 and -113 ppm, respectively, showing two chemically different environments for the 2,6-difluoro substituents of the porphyrinate, presumably giving the credit to the two chemically inequivalent sides of the porphyrinate, wherein one bears the superoxo radical anion [68]. However, due to the instability of **9-THF-O₂**, upon increasing temperature to room temperature, **9-THF-O₂** decomposes to a high-spin iron(III)-hydroxide species, $[(\text{F}_8\text{TPP})\text{Fe}^{\text{III}}(\text{OH})]$ (Figure 7), with a paramagnetic ^2H NMR shift at $\delta_{\text{pyrrole}} = 125$ ppm.

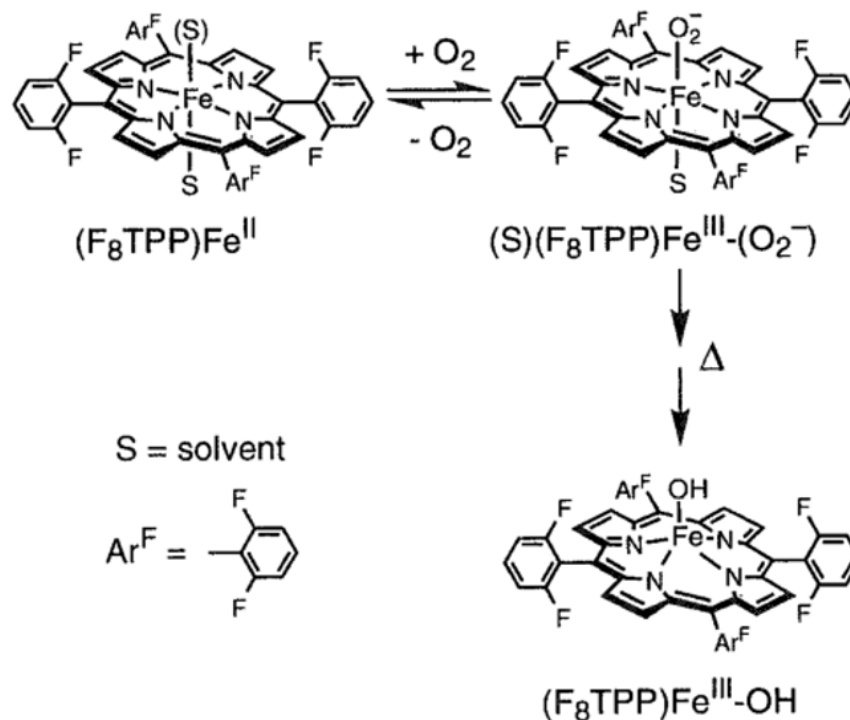


Figure 7. Formation of $[(\text{THF})(\text{F}_8\text{TPP})\text{Fe}^{\text{III}}(\text{O}_2^{\bullet-})]$ and its thermal decay to $[(\text{F}_8\text{TPP})\text{Fe}^{\text{III}}(\text{OH})]$. Reprinted with permission from Ref. [100]. Copyright 2001, American Chemical Society.

While in noncoordinating solvents, including toluene and CH_2Cl_2 , **9** reacts with O_2 to generate not an iron(III)-superoxo species, but a peroxo-bridged dinuclear complex $\{[(\text{F}_8\text{TPP})\text{Fe}^{\text{III}}]_2(\text{O}_2^{2-})\}$ at 193 K (Figure 8) [100]. The formulation of $\{[(\text{F}_8\text{TPP})\text{Fe}^{\text{III}}]_2(\text{O}_2^{2-})\}$ is further corroborated by O_2 titration of **9** in CH_2Cl_2 at 193 K, and a stoichiometry of 0.5–0.55 equiv of O_2 per equiv of $[(\text{F}_8\text{TPP})\text{Fe}^{\text{II}}]$ is determined. $\{[(\text{F}_8\text{TPP})\text{Fe}^{\text{III}}]_2(\text{O}_2^{2-})\}$ transforms into a high-spin iron(III)-hydroxide species, $[(\text{F}_8\text{TPP})\text{Fe}^{\text{III}}(\text{OH})]$ when increasing the reaction temperature.

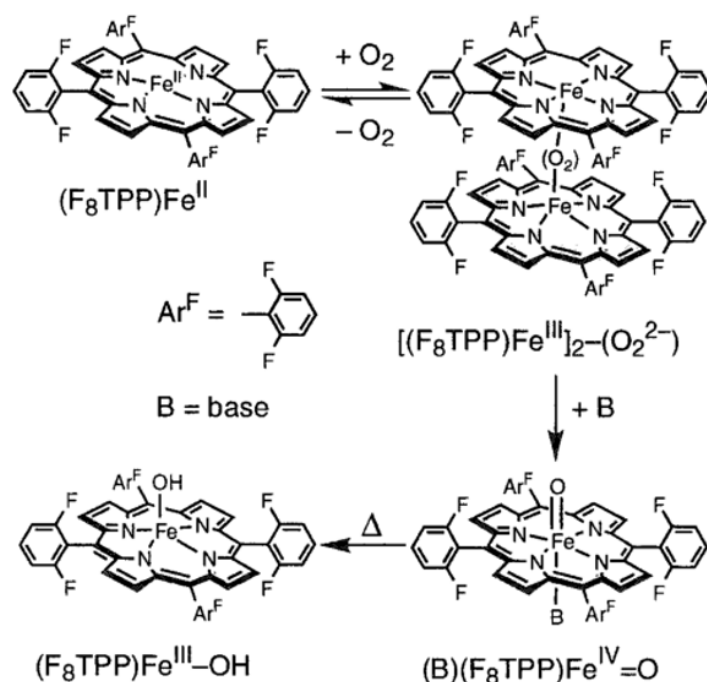


Figure 8. Formation of peroxo-bridged dinuclear complex $\{[(\text{F}_8\text{TPP})\text{Fe}^{\text{III}}]_2(\text{O}_2^{2-})\}$ in noncoordinating solvents and its stepwise transformation to a high-spin iron(III)-hydroxide species, $[(\text{F}_8\text{TPP})\text{Fe}^{\text{III}}(\text{OH})]$. Reprinted with permission from Ref. [100]. Copyright 2001, American Chemical Society.

3.4. Encapsulation of the Metalloporphyrin in Metal–Organic Frameworks (MOFs)

The aforementioned strategies to promote O_2 activation and stabilize iron- O_2 adducts involve complicated multistep organic synthesis and harsh reaction conditions, which limits the development of O_2 activation. One promising approach encapsulating the metalloporphyrin in MOFs has been used as a platform to study iron–dioxygen species. MOFs are particularly well-suited for O_2 activation because of their high degree of synthetic tunability, their porous structure, and their amenability to single-crystal diffraction studies [103,104].

Recently, Harris and co-workers reported a five-coordinate heme dioxygen adduct isolated within an MOF (Figure 9) [105]. The Zr-based porphyrinic MOF PCN-224 is metalated with iron(II) to produce a four-coordinate (4C) ferrous heme-containing complex, PCN-224 Fe^{II} (**10**). Even though some heme-containing MOFs have been synthesized [106–110], **10** is the first example of an MOF with coordinatively unsaturated ferrous heme centers. Upon exposure of single crystals of **10** to 1 atm of O_2 at -78°C , an obvious color change was observed. Its X-ray diffraction analysis reveals that an iron(III) center coordinates to superoxo moiety ($\text{PCN-224Fe}^{\text{III}}\text{O}_2^{\bullet-}$, **10-O}_2**) in an end-on η^1 geometry with Fe–O distance of 1.79(1), O–O distance of 1.15(4) Å, and Fe–O–O angle of 118° . Subsequent Mössbauer spectroscopy further demonstrates the presence of a low-spin electronic configuration for iron(III). Temperature-dependent experiments reveal stoichiometry 1:1 of Fe: O_2 and also provide insight into the energetics of dioxygen binding, giving a binding enthalpy of $-34(4)$ kJ/mol. The binding enthalpy of **10-O}_2** is notably lower than that of 6C Fe^{II} centers (-63 to -65 kJ/mol). **10-O}_2** is the only example with a structurally characterized “base-free” 5C heme-superoxo species. These results certify the solid-state structure of MOFs can provide a platform to enable isolation and thorough characterization of unstable species that can only be observed transiently in molecular form. In their subsequent works, this system is further extended to PCN-224(Co) and PCN-224(Mn), which also demonstrated selective reversible O_2 binding to generate $\text{Co}^{\text{III}}-\text{O}_2^{\bullet-}$ adduct and $\text{Mn}^{\text{IV}}-\text{O}_2^{2-}$ adduct, respectively [111,112].

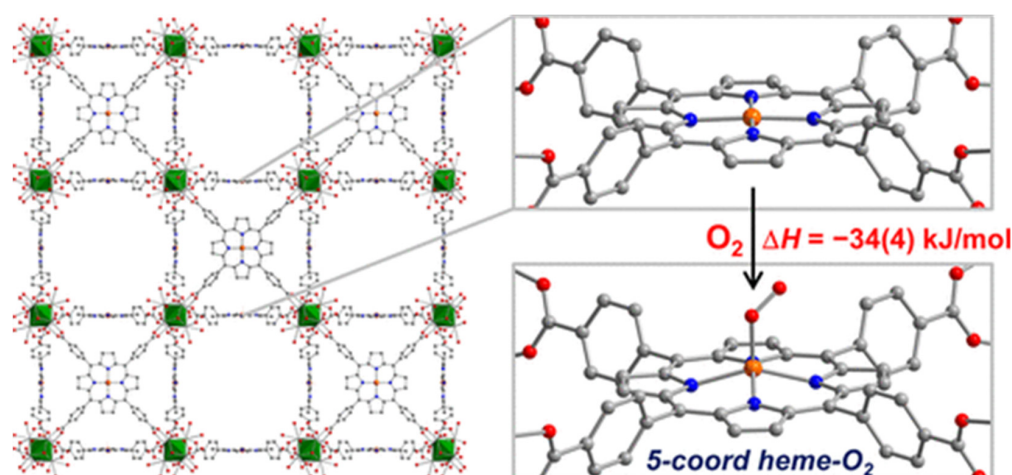


Figure 9. Reaction of porphyrinic MOF, PCN-224Fe^{II} (**10**), with O₂ at -78°C to generate the first structurally characterized 5C low-spin heme-superoxo species PCN-224Fe^{III}O₂^{•-} (**10-O₂**). Reprinted with permission from Ref. [105]. Copyright 2014, American Chemical Society.

4. Conclusions

Dioxygen activation to generate the reactive metal–oxygen species is extremely important in the context of energy storage and utilization. In nature, a variety of metalloenzymes with cheap metal active sites, such as iron, are able to activate dioxygen under ambient conditions. These systems inspire bioinorganic chemists to synthesize biomimetic small-molecule iron porphyrin complexes, which are designed to carry out the O₂ activation. However, the isolation and characterization of iron–dioxygen adducts is a big challenge because the absence of surrounding protein superstructure makes iron–dioxygen adducts unstable. The last half century has seen the development of biomimetic chemistry to overcome this challenge. From a historical standpoint, this review shows the great progress in the development of a variety of iron porphyrin models of O₂-dependent heme enzymes to interpret iron–dioxygen intermediates. Owing to increasingly sophisticated spectroscopic techniques (e.g., Mössbauer, XAS, EXAFS, EPR, rR), cryogenic temperature techniques, and porphyrin ligand development, a few iron–dioxygen species are spectroscopically observed by reacting iron porphyrin complexes with O₂. Significant sterically hindered iron porphyrin complexes with axial ligands could mimic enzymes to make metal active sites sequestered, promote O₂ binding, and increase the stability of iron–dioxygen species. Secondary coordination sphere interaction is another useful strategy to stabilize iron–dioxygen species via H-bond interactions, which helps keep iron–dioxygen species separate from each other. However, there are limits to these strategies because they involve complicated multistep organic synthesis and harsh reaction conditions. Very recently, due to the merit of MOFs—which are well-suited for O₂ activation because of their high degree of synthetic tunability, their porous structure, and their amenability to single-crystal diffraction studies—one promising approach encapsulating and separating the iron porphyrin in MOFs has been used as a platform to study iron–dioxygen species. The synthesis of MOFs is facile, and the encapsulation results in the trapping of Fe–O₂ adducts that lack a sixth axial ligand trans to the O₂ binding sites.

Metalloenzymes can efficiently catalyze O₂-dependent oxidations, but their mechanisms remain unclear. The development of synthetic models of metal–oxygen intermediates help to illustrate the enzyme mechanisms. Meanwhile, progress in the illustration of the mechanisms for the metalloenzymes guides chemists to design potent and selective catalysts. Although O₂ activation by biomimetic heme complexes has always been a focus of biomimetic chemists, there are still relatively few synthesized complexes that are capable of activating O₂ so far, and the oxidation yields of these few successful complexes remain poor compared with that of metalloenzymes. With the great progress being made over

the past several decades, the future holds remarkable promise in isolating metal–dioxygen intermediates in O₂ activation by metal porphyrin complexes.

Author Contributions: Conceptualization and writing, X.L.; review, S.W. and J.-H.Q. All authors have read and agreed to the published version of the manuscript.

Funding: This research was funded by the National Natural Science Foundation of China (Grants 22102068 and 22105093) and Key Scientific Research Projects of Higher Education of He'nan Province (Grants 22A150016 and 22A150049).

Institutional Review Board Statement: Not applicable.

Informed Consent Statement: Not applicable.

Data Availability Statement: Not applicable.

Conflicts of Interest: The authors declare no conflict of interest.

References

1. Kovaleva, E.G.; Lipscomb, J.D. Versatility of Biological Non Heme Fe(II) Centers in Oxygen Activation Reactions. *Nat. Chem. Biol.* **2008**, *4*, 186–193. [[CrossRef](#)] [[PubMed](#)]
2. Guo, M.; Corona, T.; Ray, K.; Nam, W. Heme and Nonheme High-Valent Iron and Manganese Oxo Cores in Biological and Abiological Oxidation Reactions. *ACS Cent. Sci.* **2019**, *5*, 13–28. [[CrossRef](#)] [[PubMed](#)]
3. Pau, M.Y.M.; Lipscomb, J.D.; Solomon, E.I. Substrate activation for O₂ reactions by oxidized metal centers in biology. *Proc. Natl. Acad. Sci. USA* **2007**, *104*, 18355–18362. [[CrossRef](#)]
4. Kovacs, J.A. How Iron Activates O₂. *Science* **2003**, *299*, 1024–1025. [[CrossRef](#)]
5. Sawyer, D.T. *Oxygen Chemistry*; Oxford University Press: New York, NY, USA, 1991.
6. Nam, W. Dioxygen Activation by Metalloenzymes and Models. *Acc. Chem. Res.* **2007**, *40*, 465. [[CrossRef](#)]
7. Zaragoza, J.P.T.; Goldberg, D.P. Dioxygen Binding and Activation Mediated by Transition Metal Porphyrinoid Complexes. In *Dioxygen-Dependent Heme Enzymes*; The Royal Society of Chemistry: London, UK, 2018; pp. 1–36.
8. Ortiz de Montellano, P.R. Hydrocarbon Hydroxylation by Cytochrome P450 Enzymes. *Chem. Rev.* **2010**, *110*, 932–948. [[CrossRef](#)]
9. McQuarters, A.B.; Wolf, M.W.; Hunt, A.P.; Lehnert, N. 1958–2014: After 56 years of research, cytochrome P450 reactivity is finally explained. *Angew. Chem. Int. Ed.* **2014**, *53*, 4750–4752. [[CrossRef](#)]
10. Denisov, I.G.; Makris, T.M.; Sligar, S.G.; Schlichting, I. Structure and Chemistry of Cytochrome P450. *Chem. Rev.* **2005**, *105*, 2253–2278. [[CrossRef](#)]
11. Huang, X.; Groves, J.T. Beyond ferryl-mediated hydroxylation: 40 years of the rebound mechanism and C–H activation. *J. Biol. Inorg. Chem.* **2017**, *22*, 185–207. [[CrossRef](#)]
12. Noh, H.; Cho, J. Synthesis, characterization and reactivity of non-heme 1st row transition metal-superoxo intermediates. *Coord. Chem. Rev.* **2019**, *382*, 126–144. [[CrossRef](#)]
13. Huang, X.; Groves, J.T. Oxygen Activation and Radical Transformations in Heme Proteins and Metalloporphyrins. *Chem. Rev.* **2018**, *118*, 2491–2553. [[CrossRef](#)] [[PubMed](#)]
14. Fukuzumi, S.; Karlin, K.D. Kinetics and thermodynamics of formation and electron-transfer reactions of Cu–O₂ and Cu₂–O₂ complexes. *Coord. Chem. Rev.* **2013**, *257*, 187–195. [[CrossRef](#)] [[PubMed](#)]
15. Adam, S.M.; Wijeratne, G.B.; Rogler, P.J.; Diaz, D.E.; Quist, D.A.; Liu, J.J.; Karlin, K.D. Synthetic Fe/Cu Complexes: Toward Understanding Heme-Copper Oxidase Structure and Function. *Chem. Rev.* **2018**, *118*, 10840–11022. [[CrossRef](#)] [[PubMed](#)]
16. Nam, W.; Lee, Y.-M.; Fukuzumi, S. Hydrogen Atom Transfer Reactions of Mononuclear Nonheme Metal–Oxygen Intermediates. *Acc. Chem. Res.* **2018**, *51*, 2014–2022. [[CrossRef](#)]
17. Solomon, E.I.; Stahl, S.S. Introduction: Oxygen Reduction and Activation in Catalysis. *Chem. Rev.* **2018**, *118*, 2299–2301. [[CrossRef](#)]
18. Elwell, C.E.; Gagnon, N.L.; Neisen, B.D.; Dhar, D.; Spaeth, A.D.; Yee, G.M.; Tolman, W.B. Copper–Oxygen Complexes Revisited: Structures, Spectroscopy, and Reactivity. *Chem. Rev.* **2017**, *117*, 2059–2107. [[CrossRef](#)]
19. Pegis, M.L.; Wise, C.F.; Martin, D.J.; Mayer, J.M. Oxygen Reduction by Homogeneous Molecular Catalysts and Electrocatalysts. *Chem. Rev.* **2018**, *118*, 2340–2391. [[CrossRef](#)]
20. Sankaralingam, M.; Lee, Y.-M.; Nam, W.; Fukuzumi, S. Amphoteric reactivity of metal–oxygen complexes in oxidation reactions. *Coord. Chem. Rev.* **2018**, *365*, 41–59. [[CrossRef](#)]
21. Baglia, R.A.; Zaragoza, J.P.T.; Goldberg, D.P. Biomimetic Reactivity of Oxygen-Derived Manganese and Iron Porphyrinoid Complexes. *Chem. Rev.* **2017**, *117*, 13320–13352. [[CrossRef](#)]
22. Jasniewski, A.J.; Que, L., Jr. Dioxygen Activation by Nonheme Diiron Enzymes: Diverse Dioxygen Adducts, High-Valent Intermediates, and Related Model Complexes. *Chem. Rev.* **2018**, *118*, 2554–2592. [[CrossRef](#)]
23. Nam, W. Synthetic mononuclear nonheme iron–oxygen intermediates. *Acc. Chem. Res.* **2015**, *48*, 2415–2423. [[CrossRef](#)]
24. Hong, S.; Lee, Y.-M.; Ray, K.; Nam, W. Dioxygen activation chemistry by synthetic mononuclear nonheme iron, copper and chromium complexes. *Coord. Chem. Rev.* **2017**, *334*, 25–42. [[CrossRef](#)]

25. Zhang, W.; Lai, W.; Cao, R. Energy-Related Small Molecule Activation Reactions: Oxygen Reduction and Hydrogen and Oxygen Evolution Reactions Catalyzed by Porphyrin- and Corrole-Based Systems. *Chem. Rev.* **2017**, *117*, 3717–3797. [[CrossRef](#)] [[PubMed](#)]
26. Natri, F.; Chino, M.; Maglio, O.; Bhagi-Damodaran, A.; Lu, Y.; Lombardi, A. Design and engineering of artificial oxygen-activating metalloenzymes. *Chem. Soc. Rev.* **2016**, *45*, 5020–5054. [[CrossRef](#)] [[PubMed](#)]
27. Sacramento, J.J.D.; Albert, T.; Siegler, M.; Moënné-Loccoz, P.; Goldberg, D.P. An Iron (III) Superoxide Corrole from Iron (II) and Dioxygen. *Angew. Chem., Int. Ed.* **2022**, *61*, e202111492. [[CrossRef](#)]
28. Ray, K.; Pfaff, F.F.; Wang, B.; Nam, W. Status of Reactive Non-Heme Metal–Oxygen Intermediates in Chemical and Enzymatic Reactions. *J. Am. Chem. Soc.* **2014**, *136*, 13942–13958. [[CrossRef](#)]
29. Fukuzumi, S.; Lee, Y.-M.; Nam, W. Structure and reactivity of the first-row d-block metal-superoxo complexes. *Dalton Trans.* **2019**, *48*, 9469–9489. [[CrossRef](#)]
30. Zhang, X.-P.; Chandra, A.; Lee, Y.-M.; Cao, R.; Ray, K.; Nam, W. Transition metal-mediated O–O bond formation and activation in chemistry and biology. *Chem. Soc. Rev.* **2021**, *50*, 4804–4811. [[CrossRef](#)]
31. Cho, J.; Sarangi, R.; Nam, W. Mononuclear Metal–O₂ Complexes Bearing Macrocyclic N-Tetramethylated Cyclam Ligands. *Acc. Chem. Res.* **2012**, *45*, 1321–1330. [[CrossRef](#)]
32. Winslow, C.; Lee, H.B.; Field, M.J.; Teat, S.J.; Rittle, J. Structure and Reactivity of a High-Spin, Nonheme Iron(III)-Superoxo Complex Supported by Phosphinimide Ligands. *J. Am. Chem. Soc.* **2021**, *143*, 13686–13693. [[CrossRef](#)]
33. Hong, S.; Sutherlin, K.D.; Park, J.; Kwon, E.; Siegler, M.A.; Solomon, E.I.; Nam, W. Crystallographic and spectroscopic characterization and reactivities of a mononuclear non-haem iron (III)-superoxo complex. *Nat. Commun.* **2014**, *5*, 5440. [[CrossRef](#)] [[PubMed](#)]
34. Mondal, P.; Ishigami, I.; Gérard, E.F.; Lim, C.; Yeh, S.R.; de Visser, S.P.; Wijeratne, G.B. Proton-coupled electron transfer reactivities of electronically divergent heme superoxide intermediates: A kinetic, thermodynamic, and theoretical study. *Chem. Sci.* **2021**, *12*, 8872–8883. [[CrossRef](#)] [[PubMed](#)]
35. Pan, H.R.; Chen, H.J.; Wu, Z.H.; Ge, P.; Ye, S.; Lee, G.H.; Hsu, H.F. Structural and Spectroscopic Evidence for a Side-on Fe (III)–Superoxo Complex Featuring Discrete O–O Bond Distances. *JACS Au* **2021**, *1*, 1389–1398. [[CrossRef](#)]
36. Lu, X.; Lee, Y.-M.; Sankaralingam, M.; Fukuzumi, S.; Nam, W. Catalytic four-electron reduction of dioxygen by ferrocene derivatives with a nonheme iron(III) TAML complex. *Inorg. Chem.* **2020**, *59*, 18010–18017. [[CrossRef](#)] [[PubMed](#)]
37. Sankaralingam, M.; Lee, Y.-M.; Lu, X.; Vardhaman, A.K.; Nam, W.; Fukuzumi, S. Autocatalytic dioxygen activation to produce an iron (V)-oxo complex without any reductants. *Chem. Commun.* **2017**, *53*, 8348–8351. [[CrossRef](#)] [[PubMed](#)]
38. Sono, M.; Roach, M.P.; Coulter, E.D.; Dawson, J.H. Heme-Containing Oxygenases. *Chem. Rev.* **1996**, *96*, 2841–2888. [[CrossRef](#)]
39. Mansuy, D.; Battioni, P. *The Porphyrin Handbook*; Kadish, K.M., Smith, J.M., Guilard, R., Eds.; Academic Press: San Diego, CA, USA, 2000; Volume 4, pp. 1–15.
40. Poulos, T.L. Heme Enzyme Structure and Function. *Chem. Rev.* **2014**, *114*, 3919–3962. [[CrossRef](#)]
41. Pauling, L. Nature of the Iron–Oxygen Bond in Oxy-haemoglobin. *Nature* **1964**, *203*, 182–183. [[CrossRef](#)]
42. Pauling, L.; Coryell, C.D. The Magnetic Properties and Structure of Hemoglobin, Oxyhemoglobin and Carbonmonoxyhemoglobin. *Proc. Natl. Acad. Sci. USA* **1936**, *22*, 210–216. [[CrossRef](#)]
43. Shaanan, B. The Iron–Oxygen Bond in Human Oxy-haemoglobin. *Nature* **1982**, *296*, 683–684. [[CrossRef](#)]
44. Collman, J.P.; Gagne, R.R.; Reed, C.A.; Robinson, W.T.; Rodley, G.A. Structure of an Iron(II) Dioxygen Complex; A Model for Oxygen Carrying Hemeproteins. *Proc. Natl. Acad. Sci. USA* **1974**, *71*, 1326–1329. [[CrossRef](#)]
45. Wilson, S.A.; Kroll, T.; Decreau, R.A.; Hocking, R.K.; Lundberg, M.; Hedman, B.; Hodgson, K.O.; Solomon, E.I. Iron L-Edge X-ray Absorption Spectroscopy of Oxy-Picket Fence Porphyrin: Experimental Insight into Fe–O₂ Bonding. *J. Am. Chem. Soc.* **2013**, *135*, 1124–1136. [[CrossRef](#)] [[PubMed](#)]
46. Weiss, J.J. Nature of the Iron–Oxygen Bond in Oxy-haemoglobin. *Nature* **1964**, *202*, 83–84. [[CrossRef](#)]
47. Lang, G.; Marshali, W. Mössbauer Effect in Some Haemoglobin Compounds. *Proc. Phys. Soc.* **1966**, *87*, 3–34. [[CrossRef](#)]
48. Sharrock, M.; Debrunner, P.G.; Schulz, C.; Lipscomb, J.D.; Marshall, V.; Gunsalus, I.C. Cytochrome P450 cam and Its Complexes, Mössbauer Parameters of the Heme Iron. *Biochim. Biophys. Acta Protein Struct.* **1976**, *420*, 8–26. [[CrossRef](#)]
49. Collman, J.P.; Brauman, J.I.; Halbert, T.R.; Suslick, K.S. Nature of O₂ and CO binding to metalloporphyrins and heme proteins. *Proc. Natl. Acad. Sci. USA* **1976**, *73*, 3333–3337. [[CrossRef](#)]
50. Yamamoto, T.; Palmer, G.; Gill, D.; Salmeen, I.T.; Rimai, L. The Valence and Spin State of Iron in Oxyhemoglobin as Inferred from Resonance Raman Spectroscopy. *J. Biol. Chem.* **1973**, *248*, 5211–5213. [[CrossRef](#)]
51. Das, T.K.; Couture, M.; Ouellet, Y.; Guertin, M.; Rousseau, D.L. Simultaneous Observation of the O–O and Fe–O₂ Stretching Modes in Oxyhemoglobins. *Proc. Natl. Acad. Sci. USA* **2001**, *98*, 479–484. [[CrossRef](#)]
52. Spiro, T.G.; Streckas, T.C. Resonance Raman Spectra of Heme Proteins. Effects of Oxidation and Spin State. *J. Am. Chem. Soc.* **1974**, *96*, 338–345. [[CrossRef](#)]
53. Goddard, W.A.; Olafson, B.D. Ozone Model for Bonding of an O₂ to Heme in Oxyhemoglobin. *Proc. Natl. Acad. Sci. USA* **1975**, *72*, 2335–2339. [[CrossRef](#)]
54. McClure, D.S. Electronic Structure of Transition-Metal Complex Ions. *Radiat. Res. Suppl.* **1960**, *2*, 218–242. [[CrossRef](#)]
55. Harcourt, R.D. Comment on a CASSCF Study of the Fe–O₂ Bond in a Dioxygen Heme Complex. *Chem. Phys. Lett.* **1990**, *167*, 374–377. [[CrossRef](#)]

56. Harcourt, R.D. Increased-Valence Formulae and the Bonding of Oxygen to Haemoglobin. *Int. J. Quantum Chem.* **1971**, *5*, 479–495. [[CrossRef](#)]
57. Schuth, N.; Mebs, S.; Huwald, D.; Wrzolek, P.; Schwalbe, M.; Hemschemeier, A.; Haumann, M. Effective Intermediate-Spin Iron in O₂-Transporting Heme Proteins. *Proc. Natl. Acad. Sci. USA* **2017**, *114*, 8556–8561. [[CrossRef](#)] [[PubMed](#)]
58. Chen, H.; Ikeda-Saito, M.; Shaik, S. Nature of the Fe–O₂ Bonding in Oxy-Myoglobin: Effect of the Protein. *J. Am. Chem. Soc.* **2008**, *130*, 14778–14790. [[CrossRef](#)]
59. Wilson, S.A.; Green, E.; Mathews, I.I.; Benfatto, M.; Hodgson, K.O.; Hedman, B.; Sarangi, R. X-ray Absorption Spectroscopic Investigation of the Electronic Structure Differences in Solution and Crystalline Oxyhemoglobin. *Proc. Natl. Acad. Sci. USA* **2013**, *110*, 16333–16338. [[CrossRef](#)]
60. Collman, J.P. Synthetic Models for the Oxygen-Binding Hemoproteins. *Acc. Chem. Res.* **1977**, *10*, 265–272. [[CrossRef](#)]
61. Farrell, N.; Dolphin, D.H.; James, B.R. Reversible Binding of Dioxygen to Ruthenium(II) Porphyrins. *J. Am. Chem. Soc.* **1978**, *100*, 324–326. [[CrossRef](#)]
62. Mak, P.J.; Thammawichai, W.; Wiedenhoef, D.; Kincaid, J.R. Resonance Raman Spectroscopy Reveals pH-Dependent Active Site Structural Changes of Lactoperoxidase Compound 0 and Its Ferryl Heme O–O Bond Cleavage Products. *J. Am. Chem. Soc.* **2015**, *137*, 349–361. [[CrossRef](#)]
63. Unno, M.; Chen, H.; Kusama, S.; Shaik, S.; Ikeda-Saito, M. Structural Characterization of the Fleeting Ferric Peroxo Species in Myoglobin: Experiment and Theory. *J. Am. Chem. Soc.* **2007**, *129*, 13394–13395. [[CrossRef](#)]
64. Kuhnel, K.; Derat, E.; Terner, J.; Shaik, S.; Schlichting, I. Structure and Quantum Chemical Characterization of Chloroperoxidase Compound 0, a Common Reaction Intermediate of Diverse Heme Enzymes. *Proc. Natl. Acad. Sci. USA* **2007**, *104*, 99–104. [[CrossRef](#)]
65. Kudrik, E.V.; Afanasiev, P.; Alvarez, L.X.; Blondin, G.; Clémancey, M.; Latour, J.-M.; Bouchu, D.; Albrieux, F.; Nefedov, S.E.; Sorokin, A.B. An N-bridged high-valent diiron–oxo species on a porphyrin platform that can oxidize methane. *Nat. Chem.* **2012**, *4*, 1024–1029. [[CrossRef](#)] [[PubMed](#)]
66. Sorokin, A.B. Phthalocyanine Metal Complexes in Catalysis. *Chem. Rev.* **2013**, *113*, 8152–8191. [[CrossRef](#)] [[PubMed](#)]
67. Sorokin, A.B. Recent progress on exploring μ -oxo bridged binuclear porphyrinoid complexes in catalysis and material science. *Coord. Chem. Rev.* **2019**, *389*, 141–160. [[CrossRef](#)]
68. Sahu, S.; Goldberg, D.P. Activation of Dioxygen by Iron and Manganese Complexes: A Heme and Nonheme Perspective. *J. Am. Chem. Soc.* **2016**, *138*, 11410–11428. [[CrossRef](#)]
69. Balch, A.L.; Chan, Y.W.; Cheng, R.J.; Lamar, G.N.; Latosgrazynski, L.; Renner, M.W. Oxygenation Patterns for Iron(II) Porphyrins. Peroxo and Ferryl (Fe^{IV}O) Intermediates Detected by Proton Nuclear Magnetic Resonance Spectroscopy during the Oxygenation of (tetramesitylporphyrin)iron(II). *J. Am. Chem. Soc.* **1984**, *106*, 7779–7785. [[CrossRef](#)]
70. Chin, D.-H.; Balch, A.L.; Lamar, G.N. Formation of porphyrin ferryl (FeO²⁺) complexes through the addition of nitrogen bases to peroxo-bridged iron (III) porphyrins. *J. Am. Chem. Soc.* **1980**, *102*, 1446–1448. [[CrossRef](#)]
71. Chin, D.-H.; Lamar, G.N.; Balch, A.L. Mechanism of autoxidation of iron(II) porphyrins. Detection of a peroxo-bridged iron(III) porphyrin dimer and the mechanism of its thermal decomposition to the oxo-bridged iron(III) porphyrin dimer. *J. Am. Chem. Soc.* **1980**, *102*, 4344–4350. [[CrossRef](#)]
72. Chin, D.-H.; Lamar, G.N.; Balch, A.L. Role of ferryl (FeO²⁺) complexes in oxygen atom transfer reactions. Mechanism of iron (II) porphyrin catalyzed oxygenation of triphenylphosphine. *J. Am. Chem. Soc.* **1980**, *102*, 5945–5947. [[CrossRef](#)]
73. Collman, J.P.; Boulatov, R.; Sunderland, C.J.; Fu, L. Functional analogues of cytochrome *c* oxidase, myoglobin, and hemoglobin. *Chem. Rev.* **2004**, *104*, 561–588. [[CrossRef](#)]
74. Momenteau, M.; Reed, C.A. Synthetic Heme Dioxygen Complexes. *Chem. Rev.* **1994**, *94*, 659–698. [[CrossRef](#)]
75. Suslick, K.S.; Reinert, T.J. The synthetic analogs of O₂-binding heme proteins. *J. Chem. Educ.* **1985**, *62*, 974. [[CrossRef](#)]
76. Collman, J.P.; Fu, L. Synthetic models for hemoglobin and myoglobin. *Acc. Chem. Res.* **1999**, *32*, 455–463. [[CrossRef](#)]
77. Collman, J.P.; Gagne, R.R.; Halbert, T.R.; Marchon, J.-C.; Reed, C.A. Reversible Oxygen Adduct Formation in Ferrous Complexes Derived from a “Picket Fence” Porphyrin. *A Model for Oxymyoglobin*. *J. Am. Chem. Soc.* **1973**, *95*, 7868–7870. [[CrossRef](#)] [[PubMed](#)]
78. Jameson, G.B.; Rodley, G.A.; Robinson, W.T.; Gagne, R.R.; Reed, C.A.; Collman, J.P. Structure of a dioxygen adduct of (1-methylimidazole)-meso-tetrakis(α,α,α -*o*-pivalamidophenyl)porphyrinatoiron(II). An iron dioxygen model for the heme component of oxymyoglobin. *Inorg. Chem.* **1978**, *17*, 850–857. [[CrossRef](#)]
79. Yeh, C.-Y.; Chang, C.J.; Nocera, D.G. “Hangman” porphyrins for the assembly of a model heme water channel. *J. Am. Chem. Soc.* **2001**, *123*, 1513–1514. [[CrossRef](#)]
80. Schappacher, M.; Ricard, L.; Fischer, J.; Weiss, R.; Bill, E.; Montiel-Montoya, R.; Winkler, H.; Trautwein, A.X. Synthesis, structure and spectroscopic properties of two models for the active site of the oxygenated state of cytochrome P540. *Eur. J. Biochem.* **1987**, *168*, 419–429. [[CrossRef](#)]
81. Cramer, C.J.; Tolman, W.B.; Theopold, K.H.; Rheingold, A.L. Variable Character of O–O and M–O Bonding in Side-on (η^2) 1:1 Metal Complexes of O₂. *Proc. Natl. Acad. Sci. USA* **2003**, *100*, 3635–3640. [[CrossRef](#)]
82. Jameson, G.B.; Molinaro, F.S.; Ibers, J.A.; Collman, J.P.; Brauman, J.I.; Rose, E.; Suslick, K.S. Structural Changes upon Oxygenation of an Iron(II)(porphyrinato)(imidazole) Complex. *J. Am. Chem. Soc.* **1978**, *100*, 6769–6770. [[CrossRef](#)]

83. Jameson, G.B.; Molinaro, F.S.; Ibers, J.A.; Collman, J.P.; Brauman, J.I.; Rose, E.; Suslick, K.S. Models for the Active Site of Oxygen-Binding Hemoproteins. Dioxygen Binding Properties and the Structures of (2-Methylimidazole)-Meso-tetra($\alpha,\alpha,\alpha,\alpha$ -o-pivalamidophenyl)porphyrinatoiron(II)-Ethanol and Its Dioxygen Adduct. *J. Am. Chem. Soc.* **1980**, *102*, 3224–3237. [[CrossRef](#)]
84. Collman, J.P.; Gagne, R.R.; Reed, C.; Halbert, T.R.; Lang, G.; Robinson, W.T. Picket fence porphyrins. Synthetic models for oxygen binding hemoproteins. *J. Am. Chem. Soc.* **1975**, *97*, 1427–1439. [[CrossRef](#)] [[PubMed](#)]
85. Collman, J.P.; Gagne, R.R.; Reed, C.A. Paramagnetic dioxygen complex of iron(II) derived from a picket fence porphyrin. Further models for hemoproteins. *J. Am. Chem. Soc.* **1974**, *96*, 2629–2631. [[CrossRef](#)] [[PubMed](#)]
86. Brault, D.; Rougee, M. Ferrous porphyrins in organic solvents. I. Preparation and coordinating properties. *Biochemistry* **1974**, *13*, 4591–4597. [[CrossRef](#)]
87. Springer, B.A.; Sligar, S.G.; Olson, J.S.; Phillips, G.N., Jr. Mechanisms of Ligand Recognition in Myoglobin. *Chem. Rev.* **1994**, *94*, 699–714. [[CrossRef](#)]
88. Traylor, T.G.; Koga, N.; Deardurff, L.A. Structural Differentiation of Carbon Monoxide and Oxygen Binding to Iron Porphyrins: Polar Pocket Effects. *J. Am. Chem. Soc.* **1985**, *107*, 6504–6510. [[CrossRef](#)]
89. Kossanyi, A.; Tani, F.; Nakamura, N.; Naruta, Y. Properties of a Binaphthyl-Bridged Porphyrin–Iron Complex Bearing Hydroxy Groups Inside Its Cavity. *Chem.-Eur. J.* **2001**, *7*, 2862–2872. [[CrossRef](#)]
90. Tani, F.; Matsu-ura, M.; Ariyama, K.; Setoyama, T.; Shimada, T.; Kobayashi, S.; Hayashi, T.; Matsuo, T.; Hisaeda, Y.; Naruta, Y. Iron Twin-Coronet Porphyrins as Models of Myoglobin and Hemoglobin: Amphibious Electrostatic Effects of Overhanging Hydroxyl Groups for Successful CO/O₂ Discrimination. *Chem.-Eur. J.* **2003**, *9*, 862–870. [[CrossRef](#)]
91. Tani, F.; Matsu-ura, M.; Nakayama, S.; Ichimura, M.; Nakamura, N.; Naruta, Y. Synthesis and Characterization of Alkanethiolate-Coordinated Iron Porphyrins and Their Dioxygen Adducts as Models for the Active Center of Cytochrome P450: Direct Evidence for Hydrogen Bonding to Bound Dioxygen. *J. Am. Chem. Soc.* **2001**, *123*, 1133–1142. [[CrossRef](#)]
92. Walters, M.A.; Spiro, T.G.; Suslick, K.S.; Collman, J.P. Resonance Raman Spectra of (Dioxygen)(porphyrinato)(hindered imidazole)iron(II) Complexes: Implications for Hemoglobin Cooperativity. *J. Am. Chem. Soc.* **1980**, *102*, 6857–6858. [[CrossRef](#)]
93. Desbois, A.; Momenteau, M.; Lutz, M. Resonance Raman Spectroscopy of iron(II) Superstructured Porphyrins: Influence of Porphyrin Distortions on Carbonyl and Dioxygen Ligand Dissociation. *Inorg. Chem.* **1989**, *28*, 825–834. [[CrossRef](#)]
94. Oertling, W.A.; Kean, R.T.; Wever, R.; Babcock, G.T. Factors Affecting the Iron-Oxygen Vibrations of Ferrous Oxy and Ferryl Oxo Heme Proteins and Model Compounds. *Inorg. Chem.* **1990**, *29*, 2633–2645. [[CrossRef](#)]
95. Walters, M.A.; Spiro, T.G. Resonance Raman Spectroscopic Studies of Axial Ligation in Oxyhemoglobin and Oxymyoglobin, and Nitrosylmyoglobin. *Biochemistry* **1982**, *21*, 6989–6995. [[CrossRef](#)]
96. Hirota, S.; Ogura, T.; Appelman, E.H.; Shinzawa-Itoh, K.; Yoshikawa, S.; Kitagawa, T. Observation of a New Oxygen-Isotope-Sensitive Raman Band for Oxyhemoproteins and Its Implications in Heme Pocket Structures. *J. Am. Chem. Soc.* **1994**, *116*, 10564–10570. [[CrossRef](#)]
97. Basolo, F.; Hoffman, B.M.; Ibers, J.A. Synthetic Oxygen Carriers of Biological Interest. *Acc. Chem. Res.* **1975**, *8*, 384–392. [[CrossRef](#)]
98. Eaton, W.A.; Henry, E.R.; Hofrichter, J.; Mozzarelli, A. Is Cooperative Oxygen Binding by Hemoglobin Really Understood? *Nat. Struct. Biol.* **1999**, *6*, 351–358. [[CrossRef](#)] [[PubMed](#)]
99. Chufán, E.E.; Karlin, K.D. An Iron–Peroxo Porphyrin Complex: New Synthesis and Reactivity Toward a Cu(II) Complex Giving a Heme–Peroxo–Copper Adduct. *J. Am. Chem. Soc.* **2003**, *125*, 16160–16161. [[CrossRef](#)] [[PubMed](#)]
100. Ghiladi, R.A.; Kretzer, R.M.; Guzei, I.; Rheingold, A.L.; Neuhold, Y.-M.; Hatwell, K.R.; Zuberbühler, A.D.; Karlin, K.D. (F₈TPP)Fe^{II}/O₂ Reactivity Studies [F₈TPP = tetrakis(2,6-difluorophenyl)porphyrinate(2–)]: Spectroscopic (UV-Visible and NMR) and Kinetic Study of Solvent-Dependent (Fe/O₂ = 1:1 or 2:1) Reversible O₂-Reduction and Ferryl Formation. *Inorg. Chem.* **2001**, *40*, 5754–5767. [[CrossRef](#)]
101. Garcia-Bosch, I.; Adam, S.M.; Schaefer, A.W.; Sharma, S.K.; Peterson, R.L.; Solomon, E.I.; Karlin, K.D. A “Naked” Fe^{III}-(O₂²⁻)-Cu^{II} Species Allows for Structural and Spectroscopic Tuning of Low-Spin Heme-Peroxo-Cu Complexes. *J. Am. Chem. Soc.* **2015**, *137*, 1032–1035. [[CrossRef](#)]
102. Kopf, M.-A.; Neuhold, Y.-M.; Zuberbühler, A.D.; Karlin, K.D. Oxo- and Hydroxo-Bridged Heme-Copper Assemblies Formed from Acid-Base or Metal-Dioxygen Chemistry. *Inorg. Chem.* **1999**, *38*, 3093–3102. [[CrossRef](#)]
103. Li, T.-T.; Dang, L.-L.; Zhao, C.-C.; Lv, Z.-Y.; Yang, X.-G.; Zhao, Y.; Zhang, S.-H. A self-sensitized Co (II)-MOF for efficient visible-light-driven hydrogen evolution without additional cocatalysts. *J. Solid State Chem.* **2021**, *304*, 122609–122614. [[CrossRef](#)]
104. Dang, L.-L.; Zhang, T.-T.; Li, T.-T.; Chen, T.; Zhao, Y.; Zhao, C.-C.; Ma, L.-F. Stable Zinc-Based Metal-Organic Framework Photocatalyst for Effective Visible-Light-Driven Hydrogen Production. *Molecules* **2022**, *27*, 1917. [[CrossRef](#)] [[PubMed](#)]
105. Anderson, J.S.; Gallagher, A.T.; Mason, J.A.; Harris, T.D. A Five-Coordinate Heme Dioxygen Adduct Isolated within a Metal–Organic Framework. *J. Am. Chem. Soc.* **2014**, *136*, 16489–16492. [[CrossRef](#)] [[PubMed](#)]
106. Qin, J.-H.; Xu, P.; Huang, Y.-D.; Xiao, L.-Y.; Lu, W.; Yang, X.-G.; Ma, L.-F.; Zang, S.-Q. High loading of Mn (II)-metalated porphyrin in a MOF for photocatalytic CO₂ reduction in gas–solid conditions. *Chem. Commun.* **2021**, *57*, 8468–8471. [[CrossRef](#)]
107. Qin, J.-H.; Zhang, H.; Sun, P.; Huang, Y.-D.; Shen, Q.; Yang, X.-G.; Ma, L.-F. Ionic liquid induced highly dense assembly of porphyrin in MOF nanosheets for photodynamic therapy. *Dalton Trans.* **2020**, *49*, 17772–17778. [[CrossRef](#)] [[PubMed](#)]
108. Hagrman, P.J.; Hagrman, D.; Zubietta, J. Solid-state coordination chemistry: The self-assembly of microporous organic–inorganic hybrid frameworks constructed from tetrapyridylporphyrin and bimetallic oxide chains or oxide clusters. *Angew. Chem., Int. Ed.* **1999**, *38*, 3165–3168. [[CrossRef](#)]

109. Zou, C.; Zhang, T.; Xie, M.-H.; Yan, L.; Kong, G.-Q.; Yang, X.-L.; Ma, A.; Wu, C.-D. Four metalloporphyrinic frameworks as heterogeneous catalysts for selective oxidation and aldol reaction. *Inorg. Chem.* **2013**, *52*, 3620. [[CrossRef](#)] [[PubMed](#)]
110. Pan, L.; Kelly, S.; Huang, X.; Li, J. Unique 2D metalloporphyrin networks constructed from iron(II) and *meso*-tetra(4-pyridyl)porphyrin. *Chem. Commun.* **2002**, 2334–2335. [[CrossRef](#)]
111. Gallagher, A.T.; Kelty, M.L.; Park, J.G.; Anderson, J.S.; Mason, J.A.; Walsh, J.P.S.; Collins, S.L.; Harris, T.D. Dioxygen binding at a four-coordinate cobaltous porphyrin site in a metal–organic framework: Structural, EPR, and O₂ adsorption analysis. *Inorg. Chem. Front.* **2016**, *3*, 536–540. [[CrossRef](#)]
112. Gallagher, A.T.; Lee, J.Y.; Kathiresan, V.; Anderson, J.S.; Hoffman, B.M.; Harris, T.D. A structurally-characterized peroxomanganese(IV)porphyrin from reversible O₂ binding within a metal–organic framework. *Chem. Sci.* **2018**, *9*, 1596–1603. [[CrossRef](#)]